PHYSICAL REVIEW B **89**, 195311 (2014)

Structure and transport properties of Cu-doped Bi_2Se_3 films

Tetsuroh Shirasawa,[1,2,*] Masato Sugiki,[1] Toru Hirahara,[3] Masaki Aitani,[3] Terufusa Shirai,[3] Shuji Hasegawa,[3] and Toshio Takahashi[1]

[1]*Institute for Solid State Physics, University of Tokyo, 5-1-5 Kashiwanoha, Kashiwa, Chiba 277-8581, Japan*

[2]*JST, PRESTO, 4-1-8 Honcho Kawaguchi, Saitama, Japan*

[3]*Department of Physics, University of Tokyo, 7-3-1 Hongo, Bunkyo-ku, Tokyo 113-0033, Japan*

(Received 5 November 2013; revised manuscript received 12 May 2014; published 28 May 2014)

Atomic structure and electronic transport properties of Cu-doped topological insulator Bi_2Se_3 ($Cu_xBi_2Se_3$) films were investigated by surface x-ray diffraction and magnetotransport measurements. We revealed that by depositing Cu on the pristine Bi_2Se_3 films at room temperature the van der Waals gap between the quintuple layers was expanded to intercalate the Cu atoms. The gap size became maximum in the doping range of $0.12 \leqslant x \leqslant 0.35$, in the same manner as the bulk superconducting $Cu_xBi_2Se_3$ crystal. The optimally doped ($x = 0.12$) film was in n type and the carrier concentration was on the order of 10^{20} cm^{-3}; that agrees with the superconducting bulk crystals and is one order of magnitude larger than the pristine Bi_2Se_3 films. The film exhibited the weak antilocalization behavior as observed in the pristine films, indicating that the strong spin-orbit coupling is maintained against the Cu doping. The room-temperature doping did not lead to the possible superconducting transition down to 0.8 K, suggesting that in addition to the electron doping, another feature, that may exist in the inhomogeneous bulk $Cu_xBi_2Se_3$ crystals synthesized at much higher temperatures, is responsible for the superconductivity.

DOI: 10.1103/PhysRevB.89.195311 PACS number(s): 61.05.cp, 68.35.Ct, 74.78.−w, 73.61.Ng

I. INTRODUCTION

Unlike the conventional band insulators, bulk eigenstates of topological insulators are characterized by the nontrivial Z_2 topological number which determines the existence of the gapless surface states within the bulk band gap. The topologically protected surface states follow a Dirac-like energy dispersion with a helical spin polarization. Possible applications of the novel electronic states have a big impact on energy-efficient devices [1,2]. In analogy to the topological insulators, the topological superconductors have the topologically protected nontrivial superconducting states. Their surface holds gapless Andreev bound states within the bulk superconducting gap [3]. Theories predict that the surface states host Majorana fermions [4]. Its realization in condensed matter has attracted significant interest because of their potential use in topologically protected "fault-tolerant" quantum computing [4,5].

The Cu-doped topological insulator $Cu_xBi_2Se_3$ ($0.1 \leqslant x \leqslant 0.3$) has been regarded as a leading candidate for the topological superconductor, after the superconducting transition below 4 K was discovered by Hor *et al.* [6]. Sasaki *et al.* claimed that the zero-energy surface Andreev bound states actually exist within the superconducting gap, based on the point-contact transport measurements [7]. However, the recent scanning tunneling microscopy/spectroscopy (STM/STS) study could not observe the in-gap state and suggested the conventional Bardeen-Cooper-Schrieffer-type isotropic superconducting state [8]. The recent transport measurement has also denied the existence of Majorana fermions [9].

The presently available $Cu_xBi_2Se_3$ crystals have an inevitable inhomogeneity and strong disorder, which would be essentially responsible for the discrepancy of the superconducting origin. In the $Cu_xBi_2Se_3$ crystal, most of the Cu atoms are considered to be intercalated into the van der Waals (vdW) gap between the quintuple layers (QL) of Bi_2Se_3 [see Fig. 1(a)], based on the lattice expansion along the layer stacking direction (c axis) [6]. The intercalated Cu is in the Cu^+ state and donates one electron to Bi_2Se_3. However, it is not obvious that the Cu-intercalated structure leads to the superconductivity because the superconducting volume fraction is only less than 20% in the $Cu_xBi_2Se_3$ crystals synthesized by the melt-growth method [6,10]. On the other hand, Kriener *et al.* utilized an electrochemical technique to incorporate Cu into a single crystal Bi_2Se_3 and achieved more than 50% superconducting volume fraction [11,12]. However, since their crystals are highly inhomogeneous and strongly disordered [8,12], the origin of the superconductivity is still not clear.

The superconducting $Cu_xBi_2Se_3$ crystals are synthesized at 850 °C for the melt-grown method [6] and more than 530 °C for the electrochemical method [12]. The high temperature treatments inevitably produce impurity subphases of various compositions in the Cu-Bi-Se system [6] and even $CuSe_2$, a conventional superconductor with the transition temperature of 2.4 K [13]. On the other hand, it was recently reported that deposition of Cu on ultrathin Bi_2Se_3 films leads to the intercalation structure, based on STM/STS and angle-resolved photoemission spectroscopy measurements [14]. Since the intercalation structure is formed even at room temperature in such ultrathin films, the formation of the impurity phases should be significantly suppressed. Therefore, it can be an appropriate system for studying the possible superconductivity of the intercalation structure.

In this paper, the structure and electronic transport properties of the Cu-doped Bi_2Se_3 films are reported. A systematic surface x-ray diffraction (SXRD) study reveals that the vdW gap of Bi_2Se_3 films is expanded by Cu and its doping concentration dependence is quite similar to the melt-grown bulk crystals. Hall effect measurements reveal that the optimally doped film is in n type with the carrier concentration of one order of magnitude larger than the native films, which is also

*sirasawa@issp.u-tokyo.ac.jp

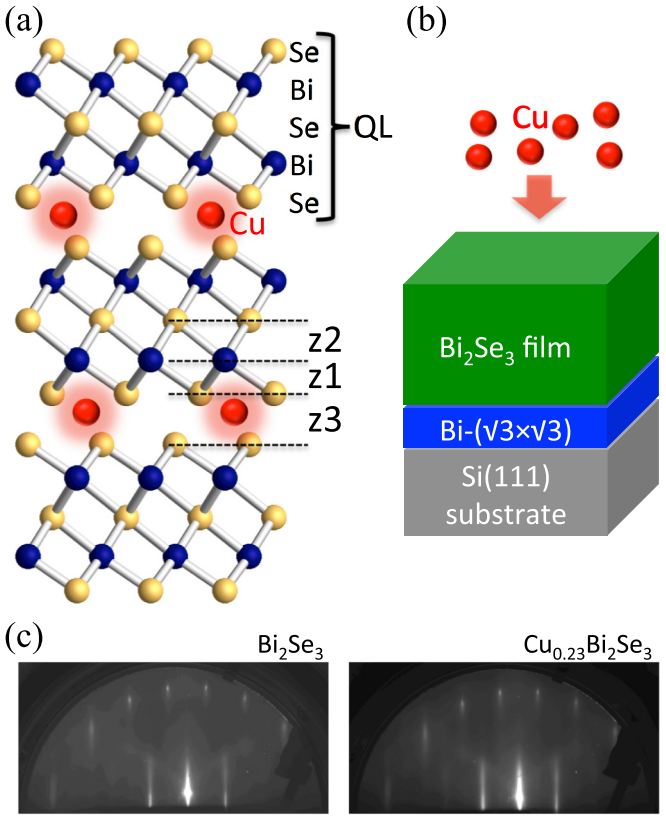

FIG. 1. (Color online) (a) Structure model of the Cu-intercalated Bi_2Se_3. (b) A schematic illustration for the deposition of Cu atoms on the Bi_2Se_3 film that is grown on Si(111) substrate with the Bi-$\sqrt{3} \times \sqrt{3}$ interface layer. (c) RHEED patterns for the pristine 6-QL Bi_2Se_3 film and the Cu-doped one.

in the same fashion as the bulk crystals. However, the possible superconducting transition was not observed down to 0.8 K in *in-situ* resistivity measurements, posing a question about the widespread picture that the simple electron doping of Bi_2Se_3 by the Cu intercalation is responsible for the superconductivity.

II. EXPERIMENTAL DETAILS

An *n*-type Si(111) wafer (1 ∼ 10 Ωcm) was used as the substrate. The substrate surface was repeatedly cleaned by resistive heating at 1250 °C until it exhibited a sharp 7 × 7 reflection high-energy electron diffraction (RHEED) pattern. We prepared a Bi-$\sqrt{3} \times \sqrt{3}$ structure on the 7 × 7 surface, that was used as a buffer layer for the growth of the high-quality Bi_2Se_3(001) film [15]. The Bi-$\sqrt{3} \times \sqrt{3}$ structure was grown by depositing Bi atoms at 450 °C. The Bi_2Se_3 films were grown on the Bi-$\sqrt{3} \times \sqrt{3}$ at 200 °C with a Se/Bi flux ratio of more than 10. Such a Se-rich condition leads to the QL-by-QL growth [15]. The thickness of the film was calibrated by the intensity oscillation of the specular RHEED spot. Cu atoms were deposited on the Bi_2Se_3 films at room temperature. The flux rate of Cu was calibrated by the Cu-induced "5 × 5" structure on Si(111), where the coverage of the "5 × 5" structure is 0.9 monolayer with respect to the topmost atomic layer of Si(111) [16]. The dopant concentration x was determined from the amount of Cu and the volume of the Bi_2Se_3 film, where the volume was estimated from the film thickness and the lattice constant $a = 4.14$ Å of Bi_2Se_3. After depositing Cu, we left the sample for 1 hour at room temperature prior to the measurements, waiting for the Cu atoms to well diffuse inside the film. No significant changes appeared in RHEED pattern upon the doping [see Fig. 1(c)].

The *in-situ* SXRD experiments were done by using a surface diffractometer equipped with an ultrahigh vacuum (UHV) chamber at beamline 15B2 of the Photon Factory at KEK. The base pressure was 1×10^{-8} Pa. Integrated scattering intensity at each point in the reciprocal space was recorded along the specular crystal truncation rod (CTR) by the rocking-scan method. The measured intensities were corrected for a scattering geometry and active sample area.

Magnetotransport measurements were *ex-situ* performed with a standard five-probe method. The probes were contacted at the edge of rectangular samples with a silver paste that was cured in ∼1 Pa at room temperature. We confirmed that the samples exposed to air exhibited clear thickness fringes in the CTR profile, indicating that the structure was not significantly damaged.

The possible superconducting transition was examined by *in-situ* resistivity measurements using the micro-four-point-probe (μ4PP) transport measurement system [17]. The spacing of the μ4PP was 200 μm. After preparing the sample, a contact between the μ4PP tip and the film surface was made *in-situ*, and the sample was cooled down to 0.8 K. The resistivity curves presented here were measured while heating the sample.

III. RESULTS AND DISCUSSION

A. Structural properties

Figure 2(a) shows the measured scattering amplitudes along the specular CTR (00 rod) for the $Cu_xBi_2Se_3$ films with $0 \leqslant x \leqslant 0.47$. The thickness of all the films was 6 QL (∼6 nm). The reciprocal lattice unit along the surface normal direction is defined by the lattice constant $c = 28.54$ Å of the nondoped Bi_2Se_3 film [18]. The Si 111, 333, and 444 Bragg peaks are located at $l = 9.10$, 27.3, and 36.4, respectively, as indicated in Fig. 2(a). All the films exhibit the similar Laue-function-like thickness fringes. An overall trend is that the amplitude of the Laue function peak becomes weaker as the dopant concentration increases, indicating a deterioration of the film quality over the doping. The degradation becomes significant above $x = 0.12$, which may be closely related to the report that when $x > 0.15$ impurity subphases are formed in the melt-grown $Cu_xBi_2Se_3$ crystals [6]. When $x = 0.47$, the film finally exhibits additional features at around $l \sim 12$ and $l \sim 25$, which may be a sign of the formation of subphases.

The positions of the Bi_2Se_3 Bragg peaks are also changed with the dopant concentration. This change becomes clearer as l increases. Figure 2(b) is a close-up view of the 0030 and 0033 Bragg peaks [dashed rectangular region of Fig. 2(a)]. The Cu-doped films have slightly smaller peak positions compared with the nondoped film, indicating the lattice expansion. The lattice constants estimated from the positions of the Bragg peaks are plotted in Fig. 2(c). The lattice expansion progresses as the dopant concentration is increased up to $x \sim 0.1$ and is saturated at a value of ∼0.23% in the range of $x = 0.12 \sim$

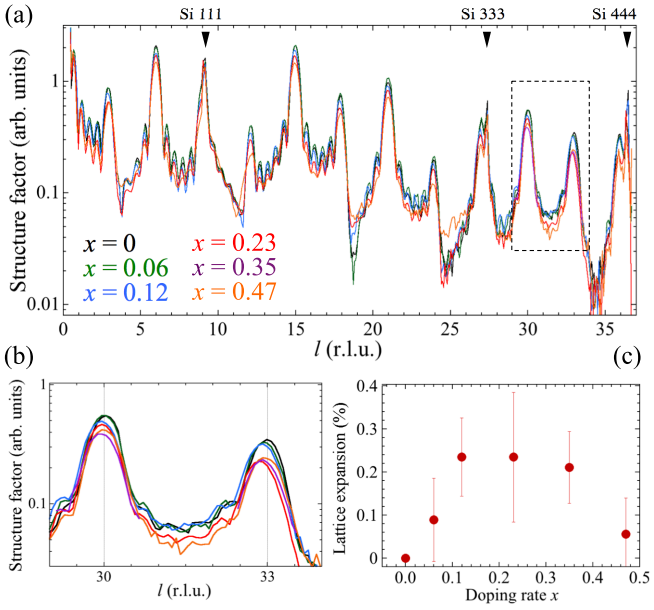

FIG. 2. (Color online) (a) The specular CTR scattering profile of the $Cu_xBi_2Se_3$ films. The criterion of the reciprocal lattice unit (r.l.u.) is the lattice constant $c = 28.54$ Å of the nondoped Bi_2Se_3 film (Ref. [18]). (b) A close-up view of the dashed rectangular region of (a). (c) The c-axis lattice expansion of the Cu-doped films with respect to the nondoped film.

0.35. The magnitude of the lattice expansion and its saturation range nicely agree with the superconducting range of the melt-grown bulk crystals [6]. Above $x = 0.12$, the structural homogeneity drops as already stated above. Therefore, from the viewpoint of structural quality and magnitude of the lattice expansion, we conclude that the optimal doping is $x \sim 0.12$, which also agrees with the bulk crystal [10]. Above the saturation range the lattice constant approaches the nondoped film, suggesting a formation of a nearly Cu-free region probably due to the phase separation.

Another prominent change in the CTR profile appears at around $l = 19$ [Fig. 3(a)]. A general feature is that the

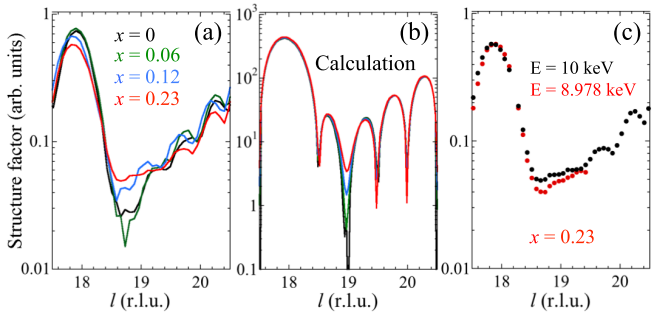

FIG. 3. (Color online) (a) A close-up view of the CTR profile of Fig. 2(a) around $l = 19$. (b) Simulated CTR profiles for the model 6-QL $Cu_xBi_2Se_3$ films, in which the doped Cu atoms occupy the middle of the vdW gap. (c) Anomalous scattering effect on the CTR profile. Red symbols are the CTR scattering amplitudes measured with an x-ray energy of 8.978 keV, which is 2 eV smaller than the Cu K absorption edge.

scattering amplitude increases with the dopant concentration. As described below, this feature indicates the existence of Cu atoms in between the vdW gap. Figure 3(b) shows simulated CTR profiles for the model structures, in which the Cu atoms occupy the middle of the vdW gap. The calculated scattering amplitudes around the dip increase with the dopant concentration, in agreement with the experimental data. The interstitial site and other intercalation sites proposed in Ref. 13 do not reproduce the feature. We further confirmed this feature by changing the effective Cu concentration for the same sample by utilizing the x-ray anomalous scattering effect [Fig. 3(c)]. We tuned the x-ray energy from 10 keV to 8.978 keV which is smaller than the Cu K-edge by 2 eV. At this energy the effective number of electron of Cu is decreased by 10 due to the dispersion correction for f'. As shown in Fig. 3(c) the scattering amplitudes are decreased by the anomalous scattering, which demonstrates that the tendency of Fig. 3(a) is not caused by the sample quality issue but by the concentration of the intercalated Cu atoms.

We performed the structure analysis for the $Cu_xBi_2Se_3$ films ($x = 0$, 0.06, 0.12, and 0.23) in order to discuss the doping effect on the atomic structure. We used the phase retrieval methods for the structure determination [19,20], because determining the structure parameters of every atom in the film is a hard task for the conventional least-squares fitting method. The structure analysis was completed satisfactorily; the calculated CTR profiles almost completely reproduce the experimental data (R factor was less than 4% for all the samples). The optimized electron densities projected on the c axis are plotted in Fig. 4(a). The origin of the axis is set at the topmost layer of the Si substrate. Above the substrate, a bunch of five peaks represents the QL, in which two tall peaks correspond to the Bi layers and the three smaller peaks to the Se layers. The electron density profiles were decomposed into Gaussian profiles, and then an atomic layer position, the number of electron, and an atomic layer width were derived from the peak potion, area, and width of the Gaussian profile, respectively [21,22]. As indicated by the arrow in Fig. 4(a), all the profiles clearly demonstrate that the Bi-$\sqrt{3} \times \sqrt{3}$ layer persists in between the Si and $Cu_xBi_2Se_3$. The mean value of the interlayer spacings between the Bi-$\sqrt{3} \times \sqrt{3}$ and the films is 3.21 ± 0.08 Å, which is much larger than the vdW gap of 2.54 Å in Bi_2Se_3 crystal, indicating a weak substrate-film interaction. The interface structure would be an important subject for building the thin-film devices and will be discussed in detail elsewhere [23].

The electron density profiles do not show the existence of the Cu visually because of its small population and random distribution [14]. However, we see a doping effect clearly on the structural modification of the Bi_2Se_3. The interlayer spacings $z1$,$z2$, and $z3$ obtained from the structure analysis are summarized in Fig. 4(b), where the definition of $z1$,$z2$, and $z3$ is given in Fig. 1(a). The dashed lines in Fig. 4(b) are the mean values of the nondoped films, and the variations from the references are plotted for the Cu-doped films. The reference values are $z = 1.56 \pm 0.04$ Å, $z2 = 1.91 \pm 0.03$ Å, and $z3 = 2.54 \pm 0.03$ Å, respectively. The most prominent feature is the expansion of the vdW gap ($z3$). On the other hand, $z1$ is slightly contracted and $z2$ is almost unchanged. Therefore, the observed overall lattice expansion [see Fig. 2(c)]

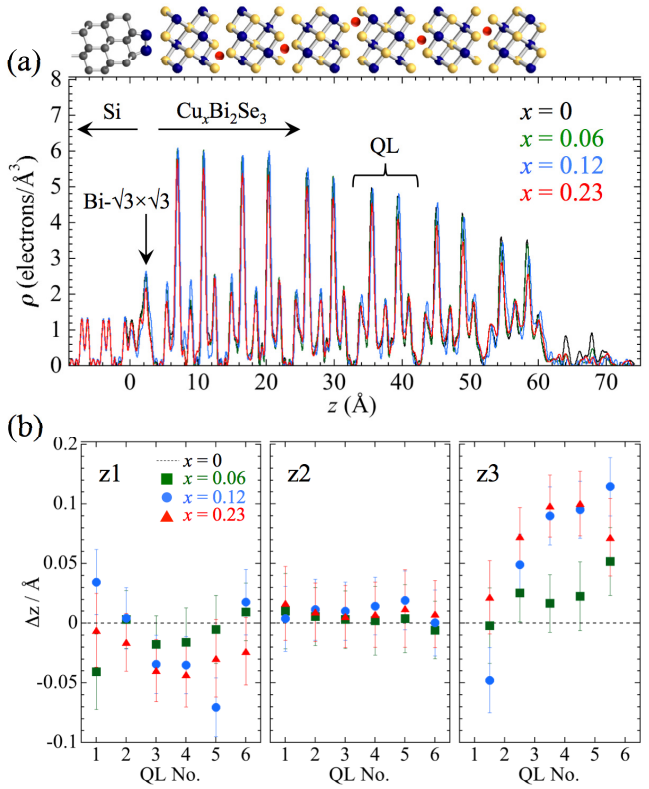

FIG. 4. (Color online) (a) The c-axis projected electron density profile of the 6-QL $Cu_xBi_2Se_3$ films. (b) Variation of the interlayer spacings $z1$,$z2$, and $z3$ for each QL of the $Cu_xBi_2Se_3$ films, where the definition of $z1$,$z2$, and $z3$ is given in Fig. 1(a). The reference values (dashed lines) are $z1 = 1.56$ Å, $z2 = 1.91$ Å, and $z3 = 2.54$ Å, which are the mean interlayer spacings of the 6-QL nondoped film.

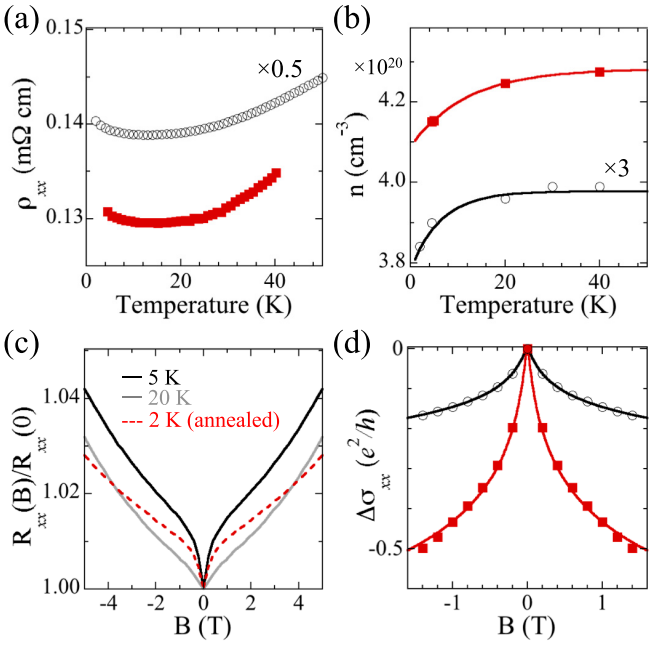

FIG. 5. (Color online) *Ex-situ* magnetotransport properties of the 8-QL $Cu_{0.12}Bi_2Se_3$ films. The filled symbols are the data from a nonannealed sample and the open symbols are from a sample annealed at 200 °C. (a) The resistivity curves. (b) The carrier density. The solid lines are the thermal activation type curves fitted to the data. (c) The magnetoresistance of the nonannealed sample at 5 K and 20 K and of the annealed sample at 2 K. (d) $\Delta\sigma_{xx}$ and the HLN fit in the weak-field range of (c).

is mainly attributed to the expansion of the vdW gap. In addition, we have already seen the indication of the Cu intercalation in Fig. 3. Therefore, it is a natural conclusion that the doped Cu atoms open the vdW gap to go into it. According to the *ab initio* calculations, other than the middle of the vdW gap, the top and bottom edges of the vdW gap can be energetically comparable intercalation sites [14]. Thus the possible random distribution through the three intercalation sites would blur the appearance of the Cu in the electron density profiles. Figure 4(b) indicates that the gap expansion decays gradually as it goes deeper into the film and almost disappears over the bottom QL. Therefore, we define the effective thickness of the Cu-doped films as ∼5 QL (∼5 nm).

B. *Ex-situ* magnetotransport properties

The magnetotransport properties of the Cu-doped films are summarized in Fig. 5. The samples are 8-QL $Cu_{0.12}Bi_2Se_3$ films, where one of them was annealed at 200 °C for 30 min trying to spread the Cu throughout the film. (We note that annealing at more than ∼230 °C caused the desorption of the film.) The results from the nonannealed and annealed samples are respectively plotted as the filled and open symbols. Figure 5(a) shows the resistivity (ρ_{xx}) curves which were measured without magnetic field. The resistivity is on the order of 10^{-1} mΩ cm, comparable to the bulk $Cu_xBi_2Se_3$ crystals [6,11] and the pristine Bi_2Se_3 films as well [24–27]. The resistivity continuously decreases as the temperature is lowered down to ∼15 K. The metallic behavior turns to the insulating one at lower temperatures. Figure 5(b) shows the carrier concentrations obtained by Hall effect measurements in which the magnetic field perpendicular to the sample surface was swept between −5 T and 5 T and the Hall coefficient R_H was determined from the slop of the ρ_{xy}-B curve. The measurements reveal that the films are in n type and the carrier concentrations are on the order of 10^{20} cm^{-3}, the same order as the bulk superconducting crystals [6,11]. The carrier concentration is increased one order of magnitude from the native Bi_2Se_3 films [24–27], in the same manner as the bulk dopings [6,11]. The carrier concentrations slightly increase above ∼15 K. The changes can be fitted by a thermal activation function $\exp\frac{E_g}{2k_BT}$ [solid curves in Fig. 5(b)] with $E_g = 2$ meV for the nonannealed sample and $E_g = 1$ meV for the annealed one. Although the origin of the activation barriers is not clear, the decrease in the carrier concentration would be mainly responsible for the increase in the resistivity below ∼15 K [Fig. 5(a)]. The Hall mobility $\mu_H = |R_H|\sigma_{xx}$ at 20 K is 170 cm^2/V for the annealed sample and 113 cm^2/V for the nonannealed sample, being the same order as the bulk superconducting crystals [6,11].

It is know that Cu acts as an ambipolar dopant in Bi_2Se_3 [28,29]; Cu locating at the intercalation site donates one

electron, while other side reactions produce defect structures such as Cu-substituted $Bi_{2-x}Cu_xSe_3$ that annihilate electrons. Assuming that all the doped Cu reside in the intercalation site, the concentration of the doped electron is calculated to be 8.5×10^{20} cm^{-3} for the $Cu_{0.12}Bi_2Se_3$. On the other hand, the measured carrier concentration of the nonannealed $Cu_{0.12}Bi_2Se_3$ film is $\sim 4.2 \times 10^{20}$ cm^{-3} [Fig. 5(b)], which indicates the existence of the defects. Based on the carrier concentration values, the population of the intercalation site is estimated to be at least $\sim$50%; since this estimation neglects the electron compensation caused by the nonintercalated Cu, the actual population should be larger than $\sim$50%. As shown in Fig. 5(b), the carrier concentration of the annealed sample is $\sim$4 times smaller than the nonannealed one, probably due to the promotion of the side reactions by the annealing. Actually, in the CTR profile $\sim$50% reduction of the Bragg peak intensity was observed after annealing at 200 °C, which directly indicates that the side reactions are activated and degrade the structural homogeneity.

Figure 5(c) shows the magnetoresistance [$R_{xx}(B)$] of the Cu-doped films. The sharp increase of the magnetoresistance in the weak-field region (~ -1 T to $\sim$1 T) is a sign of weak antilocalization (WAL) as previously observed in the native Bi_2Se_3 films [24,26,27,30,31]. This feature disappeared above 20 K. WAL effect emerges from the destructive interference for time-reversed backscattering paths from nonmagnetic impurities. In two-dimensional limit the magnetoresistance can be described by the Hikami-Larkin-Nagaoka (HLN) theory [32]

$$\Delta\sigma_{xx} = \sigma_{xx}(B) - \sigma_{xx}(0) = -\frac{\alpha e^2}{2\pi^2\hbar}\left[\log\frac{\hbar}{4eBl_\phi^2} - \psi\left(\frac{1}{2}+\frac{\hbar}{4eBl_\phi^2}\right)\right], \quad (1)$$

where B is the magnetic field, ψ is the digamma function, l_ϕ is the phase coherence length, and α is a prefactor which should be $-1/2$ in the symplectic universality class with a single conducting channel. The results of the fitting are shown in Fig. 5(d). For the nonannealed sample, even though α is fixed at $-1/2$ the experimental data are well fitted with the one parameter of $l_\phi = 130$ nm. Since in a heavily electron-doped Bi_2Se_3 the bulk carrier dominates the electronic conduction, the observed conduction channel should be the bulk one [30,31]. Therefore, it is indicated that the coherent transport stemming from the strong spin-orbit coupling of Bi_2Se_3 is maintained against the Cu doping. On the other hand, the data from the annealed sample can not be fitted without varying α. The resulting α is -0.19 with $l_\phi = 110$ nm. The significant reduction of $|\alpha|$ is likely due to the side reactions that change the electronic properties of Bi_2Se_3.

C. *In-situ* resistivity measurements for the possible superconductivity

The possible superconductivity of the Cu-doped films was investigated by the *in-situ* resistivity measurements. We measured the following five Bi_2Se_3 films with different thickness and dopant concentration, 6 QL ($x = 0.15$), 8 QL ($x = 0.25$), 12 QL ($x = 0.15$ and 0.25), and 13 QL ($x = 0.15$). A typical resistivity curve for the 13 QL ($x = 0.15$) film is shown in Fig. 6(a). The value of resistivity and the temperature dependence is comparable to those of the *ex-situ* measurements [see Fig. 5(a)], indicating that the air exposure did not significantly affect the transport property. We could not observe the superconducting transition down to the lowest achievable temperature of 0.8 K. As seen in the *ex-situ* measurements, the annealing causes the rise in the resistivity [Fig. 6(b)]. A sample annealed at $\sim$80 °C exhibited a rise in the resistivity, probably because the side reactions occur even at such a temperature mainly at step edges and domain boundaries.

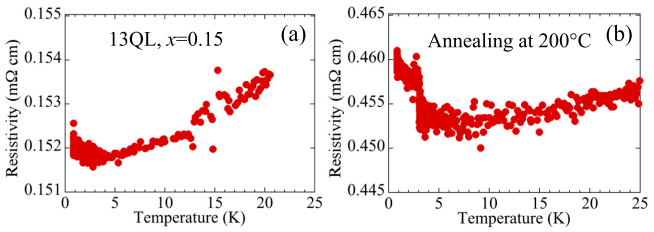

FIG. 6. (Color online) The *in-situ* resistivity curves of (a) a 13-QL $Cu_{0.15}Bi_2Se_3$ film and (b) the film annealed at 200 °C.

The nonannealed Cu-doped films had the intercalation structure and the carrier concentration that satisfies the empirical criteria of 10^{20} cm^{-3} for the emergence of the superconductivity [6,12], but the superconductivity did not appear down to 0.8 K. For this reason, first of all, we exclude the effect of the thinness of the ultrathin films, because the Cu diffusion depth of $\sim$5 nm at room temperature is not smaller than the coherence length of the superconducting state of $\xi_c = 4 \sim 5$ nm along the c-axis direction [6,33]. A probable reason is that not only the electron doping but also an additional structure, probably that is locally and randomly created in the inhomogeneous bulk crystals, is necessary for the superconductivity. As mentioned in the introduction, the bulk crystals treated at greater than $\sim$530 °C inevitably contain impurity subphases [34]. Kriener *et al.* pointed out such an inhomogeneous feature is partly responsible for the superconductivity [12]. Since the Cu-doped films were synthesized below 200 °C, the density of the impurity structure would be significantly smaller than the bulk crystals. At this stage, we do not know what kind of structure is responsible for the superconductivity. We think the formation of such a structure is difficult to control for the molecular beam epitaxy method, because the films are dewetted from the substrate by annealing at $\sim$230 °C.

IV. CONCLUSION

We characterized the structural and transport properties of the Cu-doped Bi_2Se_3 films. We found that the deposited Cu diffuses $\sim$5 nm deep into the depth and causes the expansion of the vdW gap to be intercalated even at room temperature. We determined the optimal dopant concentration of $x = 0.12$ based on the structural quality and the size of the vdW gap, which agrees with the melt-grown bulk crystal. The optimally doped Cu mainly acts as the electron donor and increases the carrier concentration one order of magnitude from the native Bi_2Se_3 films. In the film, more than 50% of

the Cu atoms are estimated to be intercalated and the carrier concentration satisfies the empirical criteria of 10^{20} cm^{-3} for the bulk superconductivity, but the film does not show the possible superconductivity down to 0.8 K. The results suggest that not only the electron doping of Bi_2Se_3 but also an additional feature, that may exist in the inhomogeneous bulk crystals synthesized at much higher temperatures, is necessary for the emergence of the superconductivity. This conclusion is consistent with the fact that the superconducting volume fraction is very small in the melt-grown bulk crystal, and it increases in the more inhomogeneous electrochemically prepared crystal.

ACKNOWLEDGMENTS

This work was supported by JSPS KAKENHI Grant No. 25246026. The SXRD experiments were done under the approval of the Photon Factory Program Advisory Committee Proposals No. 2011G654 and No. 2012G122.

[1] M. Z. Hasan and C. L. Kane, Rev. Mod. Phys. **82**, 3045 (2010).
[2] J. E. Moore, Nature (London) **464**, 194 (2010).
[3] X.-L. Qi and S.-C. Zhang, Rev. Mod. Phys. **83**, 1057 (2011).
[4] F. Wilczek, Nat. Phys. **5**, 614 (2009).
[5] A. Y. Kitaev, Ann. Phys. (Amsterdam) **303**, 2 (2003).
[6] Y. S. Hor, A. J. Williams, J. G. Checkelsky, P. Roushan, J. Seo, Q. Xu, H. W. Zandbergen, A. Yazdani, N. P. Ong, and R. J. Cava, Phys. Rev. Lett. **104**, 057001 (2010).
[7] S. Sasaki, M. Kriener, K. Segawa, K. Yada, Y. Tanaka, M. Sato, and Y. Ando, Phys. Rev. Lett. **107**, 217001 (2011).
[8] N. Levy, T. Zhang, J. Ha, F. Sharifi, A. A. Talin, Y. Kuk, and J. A. Stroscio, Phys. Rev. Lett. **110**, 117001 (2013).
[9] H. Peng, D. De, B. Lv, F. Wei, and C.-W. Chu, Phys. Rev. B **88**, 024515 (2013).
[10] L. A. Wray, S.-Y. Xu, Y. Xia, Y. S. Hor, D. Qian, A. V. Fedorov, H. Lin, A. Bansil, R. J. Cava, and M. Z. Hasan, Nat. Phys. **6**, 855 (2010).
[11] M. Kriener, K. Segawa, Z. Ren, S. Sasaki, and Y. Ando, Phys. Rev. Lett. **106**, 127004 (2011).
[12] M. Kriener, K. Segawa, Z. Ren, S. Sasaki, S. Wada, S. Kuwabata, and Y. Ando, Phys. Rev. B **84**, 054513 (2011).
[13] Y. Ando, J. Phys. Soc. Jpn. **82**, 102001 (2013).
[14] Y.-L. Wang, Y. Xu, Y.-P. Jiang, J.-W. Liu, C.-Z. Chang, M. Chen, Z. Li, C.-L. Song, L.-L. Wang, K. He, X. Chen, W.-H. Duan, Q.-K. Xue, and X.-C. Ma, Phys. Rev. B **84**, 075335 (2011).
[15] G. Zhang, H. Qin, J. Teng, J. Guo, X. Dai, Z. Fang, and K. Wu, Appl. Phys. Lett. **95**, 053114 (2009).
[16] Y. P. Zhang, K. S. Yong, H. S. O. Chan, G. Q. Xu, X. Y. Gao, D. C. Qi, X. S. Wang, and A. T. S. Wee, J. Phys. D: Appl. Phys. **41**, 095306 (2008).
[17] M. Yamada, T. Hirahara, R. Hobara, S. Hasegawa, H. Mizuno, Y. Miyatake, and T. Nagamura, e-J. Surf. Sci. Nanotech. **10**, 400 (2012).
[18] The value of the lattice constant c is slightly smaller than the bulk value of 28.64 Å. We found that the film value approaches the bulk value as the thickness increases. Details of the thickness dependent structure will be presented elsewhere.
[19] Y. Yacoby, M. Sowwan, E. Stern, J. O. Cross, D. Brewe, R. Pindak, J. Pitney, E. M. Dufresne, and R. Clarke, Nat. Mater. **1**, 99 (2002).
[20] D. K. Saldin and V. L. Shneerson, J. Phys.: Condens. Matter **20**, 304208 (2008).
[21] T. Shirasawa, M. Ohyama, W. Voegeli, and T. Takahashi, Phys. Rev. B **84**, 075411 (2011).
[22] T. Shirasawa, J. Tsunoda, T. Hirahara, and T. Takahashi, Phys. Rev. B **87**, 075449 (2013).
[23] T. Shirasawa, M. Sugiki, Y. Yamaguchi, T. Takahashi (unpublished).
[24] M. Liu, C.-Z. Chang, Z. Zhang, Y. Zhang, W. Ruan, K. He, L.-l. Wang, X. Chen, J.-F. Jia, S.-C. Zhang, Q.-K. Xue, X. Ma, and Y. Wang, Phys. Rev. B **83**, 165440 (2011).
[25] Y. S. Kim, M. Brahlek, N. Bansal, E. Edrey, G. A. Kapilevich, K. Iida, M. Tanimura, Y. Horibe, S.-W. Cheong, and S. Oh, Phys. Rev. B **84**, 073109 (2011).
[26] A. A. Taskin, S. Sasaki, K. Segawa, and Y. Ando, Phys. Rev. Lett. **109**, 066803 (2012).
[27] T. Hirahara, Y. Sakamoto, Y. Takeichi, H. Miyazaki, S.-i. Kimura, I. Matsuda, A. Kakizaki, and S. Hasegawa, Phys. Rev. B **82**, 155309 (2010).
[28] L. P. Caywood and G. R. Miller, Phys. Rev. B **2**, 3209 (1970).
[29] A. Vaško, L. Tichý, J. Horák, and J. Weissenstein, Appl. Phys. **5**, 217 (1974).
[30] H. Steinberg, J.-B. Laloë, V. Fatemi, J. S. Moodera, and P. Jarillo-Herrero, Phys. Rev. B **84**, 233101 (2011).
[31] D. Kim, P. Syers, N. P. Butch, J. Paglione, and M. S. Fuhrer, Nat. Commun. **4**, 2040 (2013).
[32] S. Hikami, A. I. Larkin, and Y. Nagaoka, Prog. Theor. Phys. **63**, 707 (1980).
[33] T. V. Bay, T. Naka, Y. K. Huang, H. Luigjes, M. S. Golden, and A. de Visser, Phys. Rev. Lett. **108**, 057001 (2012).
[34] N. Babanly, Y. Yusibov, Z. Aliev, and M. Babanly, Russ. J. Inorg. Chem. **55**, 1471 (2010).